Available online at www.sciencedirect.com
ScienceDirect
Solar Energy Materials & Solar Cells 91 (2007) 707–713
Solar Energy Materials and Solar Cells
www.elsevier.com/locate/solmat

# Analytical modelling and minority current measurements for the determination of the emitter surface recombination velocity in silicon solar cells

Santolo Daliento[a,*], Luigi Mele[a], Eugenia Bobeico[b], Laura Lancellotti[b], Pasquale Morvillo[b]

[a]*Department of Electronic Engineering and TLC, University of Naples "Federico II", Via Claudio 21, 80125 Napoli, Italy*
[b]*C.R. ENEA, Località Granatello, Portici, Italy*

Received 27 September 2006; received in revised form 19 December 2006; accepted 19 December 2006
Available online 12 February 2007

**Abstract**

A new analytical model is used to describe the emitter of silicon solar cells in order to gain information on the surface recombination velocity $S$. The procedure takes advantage of the combined use of experimental measurements, done to determine the emitter saturation current $J_{oe}$, and analytical modelling to relate $J_{oe}$ to $S$. Several experiments have been carried out on silicon solar cells having different emitter profiles subjected to various surface treatments. The influence of the surface on significant cell parameters has been analysed.


*Keywords:* Device modelling; Surface treatments

## 1. Introduction

The collection efficiency of silicon solar cells strongly depends on the carrier recombination velocity $S$ on the emitter surface. Non-passivated surfaces increase the concentration of recombination centers and then help the probability of minority carriers to be captured. The quality of silicon surfaces can be improved by depositing passivating thin films that compensate unsatisfied silicon bonds and reduce defect concentration. Unfortunately, the monitoring of the effectiveness of such processes is very difficult because of the lack of measurement techniques able to directly measure the surface recombination velocity; this is particularly true when dealing with the surface of the heavily doped region of a n/p junction, as it is the case for solar cells. On uniform doped materials an estimation of $S$ can be obtained by using optical techniques giving the measurement of the effective minority carriers lifetime $\tau_{eff}$ [1], however, as it is well known, the extraction of the surface recombination velocity from $\tau_{eff}$ is unambiguously possible only if very restrictive hypothesis can be made [2]. A direct measurement method was proposed in Ref. [3] but it requires the fabrication of a special test devices and, again, can be only applied on uniform materials.

The widely accepted method used to estimate the effectiveness of a passivating process on silicon solar cells makes use of the dependence on $S$ of the spectral response [4]; in fact, high energy photons are absorbed near the emitter surface so that the initial part of the spectral response is highly dependent on the quality of the surface. The drawback of this method is that it requires a finished solar cell and, also, sophisticated instrumentation to reveal the photoresponse.

In Ref. [5] King et al. proposed the measurement of the emitter saturation current $J_{oe}$ combined with the analytical modelling of the emitter region; it was demonstrated that, if a consistent description of the emitter region is available, the relation between $S$ and $J_{oe}$ is unique. The suitability of that procedure comes from the fact that the measurement of $J_{oe}$ does not require a finished device and can be simply done on diffused samples with a desired passivating film deposited on it [6]. The main drawback that prevents the widespread use of the method proposed in Ref. [5] is the unavailability of friendly analytical models and, also, the need for the knowledge of the emitter diffusion profile.

*Corresponding author. Tel.: +39 81 7683122; fax: +39 81 5934448.
*E-mail address:* daliento@unina.it (S. Daliento).

0927-0248/$ - see front matter © 2007 Elsevier B.V. All rights reserved.
doi:10.1016/j.solmat.2006.12.007

In Ref. [7] Cuevas et al. used a quasi-analytical model [8] to relate the minority carrier surface recombination velocity to the dopant density of the emitter region while in Ref. [9] Kerr et al. studied SiN and $SiO_2$ passivation schemes using a numerical device simulator to find the relation between $J_{oe}$ and $S$.

In this paper we propose the use of a recent [10] analytical compact solution of the transport equations in the emitter region, joined with photoconductive measurements [6], to monitor the effectiveness of several passivating processes making use of $a$-Si or $SiO_2$ depositions. Experiments have been carried out on $FZ$ substrates with different emitter doping profiles. The shape of the doping profiles have been first obtained by spreading resistance measurements, then we show that a technological process simulator, like ATHENA by Silvaco [11], can be used to perform simulated experiments that simplify the measurement procedure and whose results are consistent with truly experimental ones.

Finally, for each of the analysed devices, we use the analytical model to predict the emitter collection efficiency and we relate it to the extracted values of $S$.

## 2. Emitter modelling

A detailed description of the analytical model used in this work can be found in Ref. [10] where quantitative comments on the approximation errors are also reported. In the following we briefly recall the main analytical steps leading to the solution and we highlight how it can be used to gain information on the surface recombination velocity.

The model solves the transport equations (1) and (2) into the emitter region in the generalized case in which an illumination source, $G$, is present; the other terms of the equations have their usual meaning: $J_p$ is the hole minority current, $\tau_p$ is the minority carrier recombination lifetime, $q$ is the electron charge, $p$ is the hole density and $p_0$ is the equilibrium hole density defined as $n_{ieff}^2/N_D(x)$ where $n_{ieff}$ is the intrinsic carrier density taking into account bandgap narrowing effects, and $N_D(x)$ is the dopant density. Fig. 1 shows the structure of the high doped region in which Eqs. (1) and (2) are solved. In the appendix analytical models used to describe the dopant density dependence of the various terms are reported together with the values of the parameters we have used.

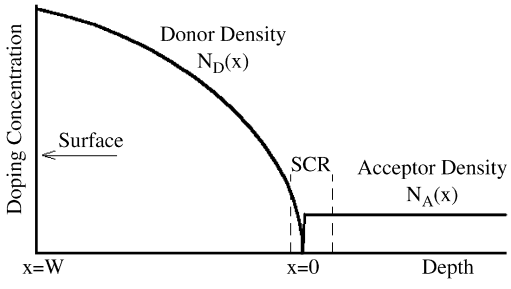


Fig. 1. Highly doped region geometry.

$$\frac{dJ_P}{dx} = -q\frac{p-p_0}{\tau_P} + qG, \tag{1}$$

$$J_P = -qD_P\frac{dp}{dx} + qD_P p\frac{d\ln p_0}{dx}. \tag{2}$$

While for dark conditions a lot of solution for Eqs. (1) and (2) exist [12], few attempts to solve the above mentioned problem have been made under illumination, and, those solutions only exist in the form of an infinite series of nested integrals [13] so that, due to the computational difficulties of their implementation, the practical applicability is very limited. Moreover, in some cases, the form of that solutions is such that the physical dependence of the solution on the relevant parameters that characterize the emitter region are not easily visible.

The closed form solution we propose reduces computational complexity and highlights the dependence on the emitter parameters. It is based on the change of variable [14]

$$y = \int_0^x \frac{d\xi}{D_P(\xi)p_0(\xi)}. \tag{3}$$

That, thanks to the definition of the normalized excess hole concentrations

$$u(x) = \frac{p-p_0}{p_0},$$

$$u' = \frac{u(x)}{u(0)}. \tag{4}$$

permits to write Eqs. (1) and (2) as follows:

$$\frac{d^2u'}{dy^2} - C_S^2u' = -C_SL_pG', \tag{5}$$

where $C_S = p_0D_p/L_p$. It has been demonstrated [15] that, if $C_S$ is constant, a closed form solution of Eq. (5) exists. Obviously, in general $C_S$ is not constant but, has it has been demonstrated for dark conditions [14], a reliable solution can be obtained by defining a proper average value. In particular, in this paper, we define for $C_S$ the average value given by

$$\overline{C_S} = \left[\frac{\int_0^w \frac{p_0(x)}{\tau_P(x)}\exp\left(-2\int_0^x \frac{d\xi}{L_P(\xi)}\right)dx}{\int_0^w \frac{1}{p_0(x)D_P(x)}\exp\left(-2\int_0^x \frac{d\xi}{L_P(\xi)}\right)dx}\right]^{1/2} \tag{6}$$

chosen with the criterion to minimize the mean square error with respect to the exact solution of Eq. (5).

In this case, the general solution of Eq. (5) is

$$u' = \cosh(\overline{C_S}y) - \phi\sinh(\overline{C_S}y) - L_pG'(y) * \sinh(\overline{C_S}y), \tag{7}$$

where $\phi$ can be determined by imposing proper boundary conditions.

From the definition of the normalized excess concentrations follows that the minority carrier current can be defined as $J' = -q\,\mathrm{d}u'/\mathrm{d}y$, and hence, from Eq. (7)

$$J'(y) = -q\left[\overline{C_S}\,\sinh(\overline{C_S}y) - \phi\overline{C_S}\cosh(\overline{C_S}y) - L_p\,\frac{\mathrm{d}}{\mathrm{d}y}\,G'(y) * \sinh(\overline{C_S}y)\right]. \tag{8}$$

The boundary conditions for this problem are

$$u'(0) = 1,$$

$$J'_P(y_w) = qS_P p(y_w)u'(y_w), \tag{9}$$

where $y_w$ is the value that the variable $y$ assumes on the emitter surface and $S_p$ is the minority carrier surface recombination velocity.

The expression of $\phi$ obtained by imposing the conditions given in Eq. (9) is

$$\phi = \frac{1 + \dfrac{\overline{C_S}}{Sp_0(w)}\tanh\left(\overline{C_S}\displaystyle\int_0^w \frac{\mathrm{d}x}{p_0(x)D(x)}\right)}{\dfrac{\overline{C_S}}{Sp_0(w)} + \tanh\left(\overline{C_S}\displaystyle\int_0^w \frac{\mathrm{d}x}{p_0(x)D(x)}\right)} \int_0^w G'(x)\frac{\sinh\left(\overline{C_S}\displaystyle\int_x^w \frac{\mathrm{d}\xi}{p_0(\xi)D(\xi)}\right)}{\cosh\left(\overline{C_S}\displaystyle\int_0^w \frac{\mathrm{d}\xi}{p_0(\xi)D(\xi)}\right)}\mathrm{d}x + \frac{\overline{C_S}}{Sp_0(w)}\int_0^w G'(x)\frac{\cosh\left(\overline{C_S}\displaystyle\int_x^w \frac{\mathrm{d}\xi}{p_0(\xi)D(\xi)}\right)}{\cosh\left(\overline{C_S}\displaystyle\int_0^w \frac{\mathrm{d}\xi}{p_0(\xi)D(\xi)}\right)}\mathrm{d}x - \frac{1}{\overline{C_S}}}{\dfrac{\overline{C_S}}{Sp_0(w)} + \tanh\left(\overline{C_S}\displaystyle\int_0^w \frac{\mathrm{d}x}{p_0(x)D(x)}\right)}. \tag{10}$$

The first term of the sum (10) does not depend on $G$ while the second term accounts for illumination. Obviously, as the second term is zero when $G$ is zero, the first term represents dark conditions.

For $y = 0$, Eq. (8) reduces to

$$J'(0) = -q\left.\frac{\mathrm{d}u'}{\mathrm{d}y}\right|_{y=0} = q\phi\overline{C_S} \tag{11}$$

and gives a compact expression for the total emitter minority current.

By using Eq. (10) we can write Eq. (11) as follows:

$$J'(0) = q\phi\overline{C_S} = q\phi_{\mathrm{dark}}\overline{C_S} - q\phi_{\mathrm{ph}}\overline{C_S} = J_{\mathrm{dark}} + J'_{\mathrm{ph}}, \tag{12}$$

where $\phi_{\mathrm{dark}}$ and $\phi_{\mathrm{ph}}$ are, respectively, the first and the second term of the sum defined in (10), $J_{\mathrm{dark}}$ is the total emitter recombination current, and $J'_{\mathrm{ph}}$ is the normalized photogenerated current.

From the above equations the most relevant emitter parameters can be easily evaluated. As an example, the emitter collection efficiency $\eta$ can be written as

$$\eta = -\frac{J_{\mathrm{ph}}}{J_{\mathrm{gen}}} = \frac{q\phi_{\mathrm{ph}}\overline{C_S}}{J_{\mathrm{gen}}}, \tag{13}$$

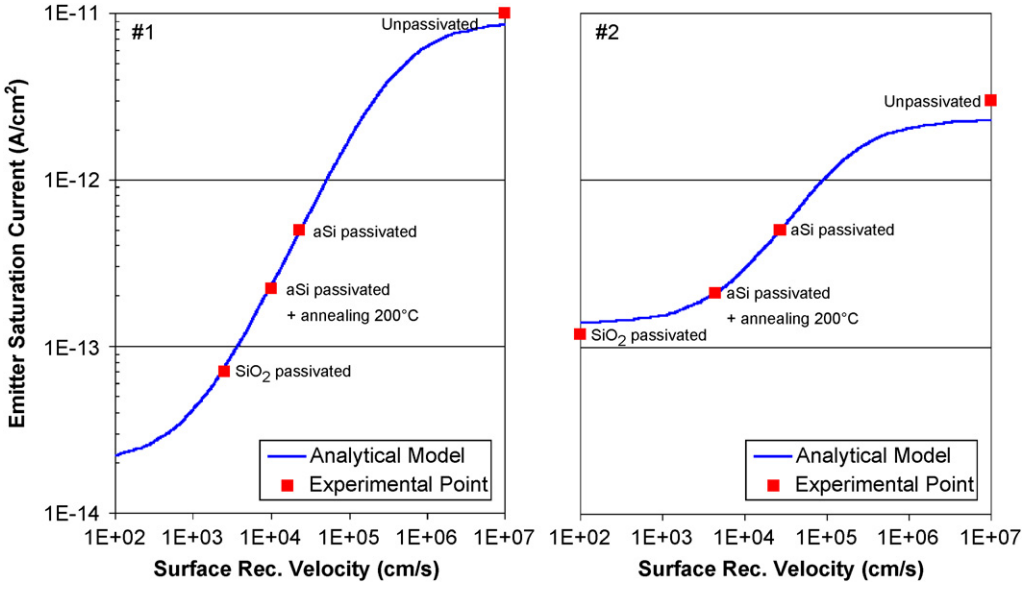


Fig. 2. Compatible couples $J_{\mathrm{oe}}$–$S$ corresponding to the doping profiles shown in Fig. 2. Experimental points are obtained by the intercepts between the measured $J_{\mathrm{oe}}$ and the analytical curves.

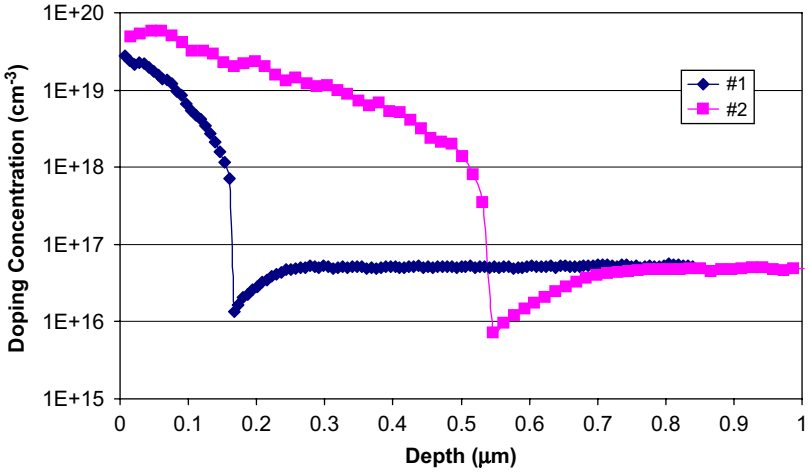


Fig. 3. Emitter doping profiles for the three samples analysed in this work. The profiles have been determined with the spreading resistance profiling technique (SRP).

where $J_{gen}$ is defined as

$$J_{gen} = q \int_0^w G(x)\,dx. \quad (14)$$

The above expression of the emitter current allows to relate $J_{oe}$ to the surface recombination velocity $S$ for each given emitter doping profile.

As an example, Fig. 2 shows the plots $J_{oe}$–$S$ obtained by solving the analytical model using as input the doping profiles shown in Fig. 3; spatially dependent models for all parameters have been used, whose details are reported in the appendix. The plots of Fig. 2 represent the possible values of $J_{oe}$ corresponding to a given value of $S$; in the next sections we enter in this plots with measured values of $J_{oe}$, obtained on samples with a known doping profile, and we extract the corresponding value of $S$, trying to relate it to some significant surface treatment made on the samples.

## 3. Experimental

Processes analysed in this work have been performed on a FZ silicon substrate with polished surfaces whose resistivity was 0.3 Ω cm. Two different emitter profiles have been tested done by means of a standard $POCl_3$ process adjusted to have junction depths of 0.2 and 0.5 μm, respectively. The results we present refer to samples labelled #1, #2, whose emitter doping profiles, measured with the spreading resistance profiling technique, are shown in Fig. 3 and whose emitter sheet resistance were 120, and 60 Ω/□, respectively.

It is important to notice that all the samples have been diffused both on the front and on the back; this is because photoconductive decay measurements done with the technique quasi steady-state photoconductive technique by Sinton et al. [6] (QSSPC ) are affected by both surfaces, hence the availability of symmetrical samples help to distinguish surface effects from bulk ones.

After the diffusion process, the two samples have been subjected to different passivating procedures using thermal oxide deposition and/or intrinsic plasma enhanced chemical vapour deposition (PECVD) amorphous silicon deposition. A summary of the various processes can be found in Table 1.

The same table also reports the emitter saturation current measured with the QSSPC technique in the various cases. The analysis of $J_{oe}$ shows, as it was expected, how this parameter is sensitive to surface condition. We note, in fact, that the current $J_{oe}$ measured on sample #1 in presence of a surface thermal oxide is very low ($7 \times 10^{-14}$ A/cm$^2$), while the same sample, analysed after etching of the oxide, presents a value of $J_{oe}$ very high ($1 \times 10^{-11}$ A/cm$^2$). These two values of $J_{oe}$ represent the upper and lower bounds found in this work and correspond to a well passivated surface and to a non passivated surface, respectively.

The third value of $J_{oe}$ reported in Table 1 for sample #1 refers to the current measured after a 350 Å amorphous silicon deposition (grown after oxide etching). As can be seen $J_{oe}$ recovers a quite low value ($5 \times 10^{-13}$ A/cm$^2$) indicating the passivating properties of $a$-Si, the effect of a thermal annealing treatment is also indicated. However, it is important to stress that, even if the comparison of $J_{oe}$ measured on the same sample with different surface treatments can give qualitative information on the effectiveness of passivating processes, the sole magnitude of $J_{oe}$ does not give any quantitative information on the actual value of the surface recombination velocity and could induce in errors in the evaluation of the reliability of passivating processes. The obvious consequence is that it is not correct to compare values of $J_{oe}$ measured on samples with different doping profiles. This point will be exploited in the next section.

Table 1
Summary of the technological processes performed on the samples analysed in this work

| | Substrate | $POCl_3$ diffusion | Dry oxidation | Oxide removal | aSi deposition | Joe ($A/cm^2$) |
|---|---|---|---|---|---|---|
| Sample #1 | FZ 0.3 Ω cm | 830 °C 10 min | 900 °C 60 min | No Oxide thickness 350 Å | No | $7\times10^{-14}$ |
| | | | | Yes | No | $1\times10^{-11}$ |
| | | | | Yes | 300 Å | $5\times10^{-13}$ |
| | | | | Yes | 300 Å +annealing 200 °C | $2.2\times10^{-13}$ |
| Sample #2 | FZ 0.3 Ω cm | 850 °C 30 mm | 850 °C 60 min +HF etching +850 °C 55 min | No Oxide thickness 180 Å | No | $1.2\times10^{-13}$ |
| | | | | Yes | No | $3.2\times10^{-12}$ |
| | | | | Yes | 300 Å | $5\times10^{-13}$ |
| | | | | Yes | 300 Å +annealing 200 °C | $2\times10^{-13}$ |

## 4. Analysis

The knowledge of the shapes of the emitter doping profiles (shown in Fig. 2) allows us to use the analytical model described in Section 2 to obtain, for each sample, all possible compatible couples of $J_{oe}$–$S$. Fig. 2 shows the curves obtained by solving the model using the emitter doping profiles measured on the two samples.

It is interesting to note how the curve referring to sample #1 shows the larger sensitivity of $J_{oe}$ with respect to the possible values of $S$. This is due to the close proximity of the surface to the emitter junction (0.2 μm) that exalts the influence of the surface conditions. The curves for sample #2 shows that, because the surface is far from the junction (0.5 μm), $J_{oe}$ is less sensitive to $S$ and depends, mainly, on bulk emitter properties.

These curves clearly show that, for different doping profiles, the same value of $J_{oe}$ could correspond to different values of $S$. In particular we note that the first two values of $J_{oe}$ reported in Table 1, referring to sample #1 with and without a passivating thermal oxide, correspond to a well passivated surface ($S<5\times10^3$ cm/s) and to a non-passivated surface ($S>10^6$ cm/s), respectively. On the other hand, the value of $J_{oe}$ found on sample #1 when an $a$-Si thin film of 300 Å has been deposited, corresponds to a value of $S$ of about $2\times10^4$ cm/s indicating a passivating effect of the $a$-Si film whose effectiveness is, however, not comparable with that of the thermal oxide. An appreciable improvement of the passivating properties of the $a$-Si, with a reduction of $S$ of about 50%, has been obtained with a subsequent thermal annealing treatment.

Actually, when a particular device is analysed, the effectiveness of a passivating process should be valued with reference to its effect on the operation of the device.

As an example, when the passivating film is part of a PV device, is also important the capability to improve the carrier collection efficiency.

This concept is well explained in Fig. 4 where, for each of the two samples, the collection efficiency, evaluated by the analytical model, is reported as a function of $S$.

From the analysis of the curve found for sample #1 we see that the collection efficiency is very high for values of $S$ up to $10^4$ cm/s, while a dramatic drop only occurs for higher $S$.

This fact seems to suggest that, in this particular case, a very effective passivating procedure is not needed as, due to the shape of the emitter region, no significant improvements of the quantum efficiency can be obtained. However, two comments are in order: first, a value of $S$ of $10^4$ cm/s on a such heavily doped surface ($5\times10^{19}$ cm$^{-3}$) can be only obtained if reliable passivation processes are made [8,9]; second, a reduction of $J_{oe}$ itself is always important as it directly contributes to the maximum allowable terminal voltage of the cell.

The analysis of Fig. 4 also shows that a completely unpassivated surface (very high $S$) is more dangerous for thinner emitter devices. This fact is an obvious consequence of the proximity of the surface to the collecting junction.

Similar results come from the analysis of $J_{oe}$ for sample #2. Again we found that thermal oxide deposition allows to achieve the better quality surface. However, it is interesting to note that the value of $J_{oe}$ measured in this case is quite different from that reported for sample #1. As already observed this is only due to the different geometries of the emitter diffusion profiles. Also in this case we found a good effectiveness of the $a$-Si deposition and a visible effect of the annealing treatment that, however, has a very small effect on the corresponding collection efficiency. In fact, Table 1 shows that $J_{oe}$ reduces of about 50%, corresponding (see Fig. 4) to values of $S$ reducing from $10^4$ cm/s (not annealed sample) to about $10^3$ cm/s (annealed sample). This reduction of $S$ correspond to an increase of the collection efficiency (extracted from Fig. 4) of about 5% only.

## 5. Process simulation

The main drawback of the technique used in this work is the need for the detailed description of the emitter doping profile. In order to overcome this limitation we have

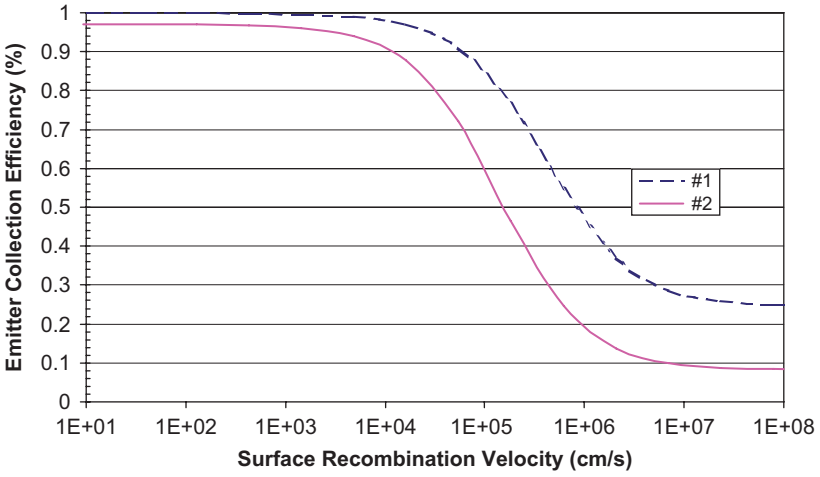


Fig. 4. Emitter collection efficiency as a function of the surface recombination velocity for sample #1, #2, evaluated by the analytical model.

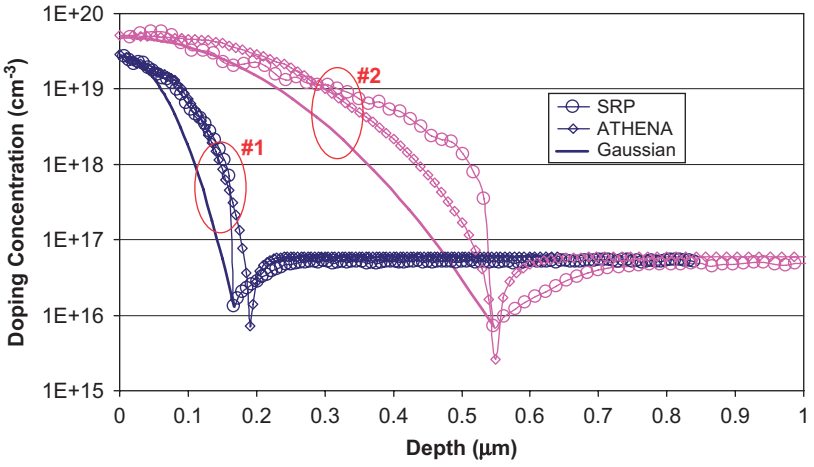


Fig. 5. Measured doping profiles (SRP) compared with simulated (ATHENA) and Gaussian shaped profiles.

checked the possibility to substitute actual profiles, obtained by means of the SRP technique, with simulated ones, obtained with the device process simulator ATHENA [11] (an evolution of the well-known program SUPREM). Process simulation is not a trivial task because requires an accurate calibration in order to gain reliable results. Together with the work presented here we have developed a calibration procedure that allows to predict the correct diffusion profile starting from the knowledge of the process parameters. Fig. 5 shows the comparison between simulated and measured emitter profiles.

As can be seen peak doping and junction depth are well defined by the process simulation while some differences exist near the kink region of the diffusion profile. This difference is acceptable from the point of view of the process simulation but could affect the prediction of $J_{oe}$. However Fig. 6, showing the comparison between the plots $J_{oe}$–$S$ obtained using the measured profiles and that obtained using the simulated ones, demonstrates that a reliable prediction is obtained using simulated data. Actually, Fig. 6 also shows the plot $J_{oe}$–$S$ obtained using the Gaussian shaped doping profiles, shown in Fig. 5, having the same peak value and the same junction depth of the measured ones; as can be seen also in this case the curve $J_{oe}$–$S$ is quite well reproduced indicating that also a simpler process simulator (able to correctly reproduce peak doping and junction depth) can give suitable results.

## 6. Conclusions

In this paper we have presented a characterization procedure that allows the monitoring of passivating processes starting from the detailed description of the emitter region. The procedure makes use of a closed form analytical solution of the transport equations in the emitter region that highlights the dependence of the emitter properties on the physical parameters affecting the cell performances. Some results on the passivating properties of both *a*-Si and $SiO_2$ films have been given. Finally, the suitability of process simulations to overcome

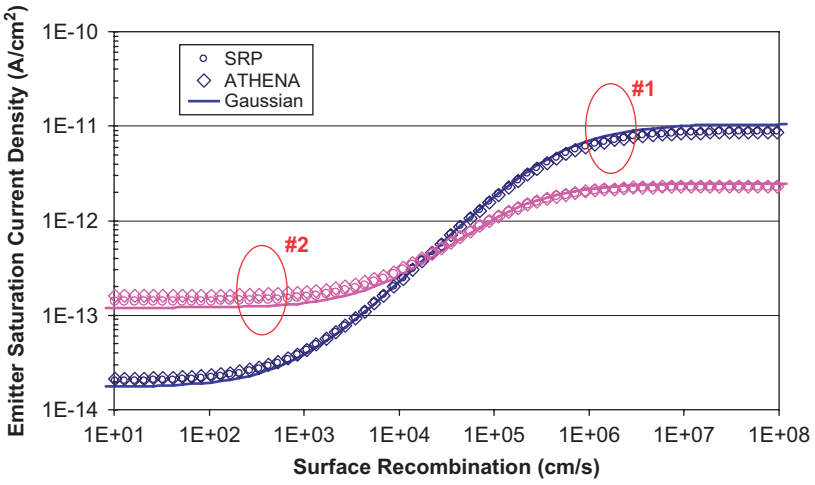


Fig. 6. Comparison between $J_{oe}$–$S$ plots obtained with measured and simulated data.

the need for expensive analysis for the measurements of the diffusion emitter profiles has been demonstrated.

**Acknowledgement**

The authors would thank Dr. Paola Delli Veneri and Dr. Lucia Mercaldo for their contribution in preparing aSi samples.

**Appendix**

Analytical models and coefficients values used in this work have been taken from the computer simulation code PC1D [16].

In particular, the mobility model has the form:

$$\mu = \mu_{\min} T_n^{\beta 1} + \frac{(\mu_{\max} - \mu_{\min}) T_n^{\beta 2}}{1 + \left( \frac{N_d(x) + N_a(x)}{N_{\text{ref}} T_n^{\beta 3}} \right)^{\alpha T_n^{\beta 4}}}$$

where $T_n$ is the temperature (K) normalized to 300 K and $\mu_{\min} = 155\,\text{cm}^2/\text{Vs}$; $\mu_{\max} = 470\,\text{cm}^2/\text{Vs}$; $\alpha = 0.9$; $\beta 1 = -0.57$; $\beta 2 = -2.23$; $\beta 3 = 2.4$; $\beta 4 = -0.146$; $N_{\text{ref}} = 10^{17}\,\text{cm}^{-3}$.

The bandgap narrowing effect is taken into account using the term $\Delta E_g$ to define the effective intrinsic carrier density

$$n_{\text{ieff}} = n_i e^{\Delta E_g / KT}$$

with

$$\Delta E_g = \text{Slope}_N \log\left( \frac{N_d}{\text{Onset}_N} \right)$$

and

$$\text{Slope}_N = 14 \times 10^{-3}\,\text{eV};$$

$$\text{Onset}_N = 1.4 \times 10^{17}\,\text{cm}^{-3};$$

Finally, the Auger coefficients used to model the recombination process are

$$C_n = 2.2 \times 10^{-31}\,\text{cm}^6/\text{s};$$

$$C_p = 9.9 \times 10^{-32}\,\text{cm}^6/\text{s}.$$

**References**

[1] K.L. Luke, L. Cheng, J. Appl. Phys. 61 (6) (1987) 2282.
[2] J. Schmidt, A.G. Aberle, J. Appl. Phys. 81 (9) (1997) 6186.
[3] S. Daliento, F. Roca, A. Sanseverino, P. Spirito, Mater. Sci. Eng. B 102 (2003) 198.
[4] H.J. Hovel, Solar Cells, Academic Press, New York, 1975.
[5] R.R. King, R.A. Sinton, R.M. Swanson, IEEE Trans. Electron. Devices 37 (2) (1990).
[6] R.A. Sinton, A. Cuevas, M. Stucking, 25th PVSC, May 1996, Washington, DC, pp. 457–460.
[7] A. Cuevas, P. Basore, G. Giroult-Matlakowski, C. Dubois, J. Appl. Phys. 80 (6) (1996) 3370.
[8] A. Cuevas, R. Merchàn, J.C. Ramos, IEEE Trans. Electron. Devices 40 (1993) 1181.
[9] M.J. Kerr, J. Schmidt, A. Cuevas, J.H. Bultman, J. Appl. Phys. 89 (7) (2001) 3821.
[10] S. Daliento, L. Mele, IEEE Trans. Electron. Devices 53 (11) (2006) 2837.
[11] ATHENA User's Manual, Silvaco International, Santa Clara, CA, 2002.
[12] A. Cuevas, M.A. Balbuena, IEEE Trans. Electron. Devices 36 (3) (1989) 553.
[13] F.J. Bisschop, L.A. Verhoef, W.C. Sinke, IEEE Trans. Electron. Devices 37 (2) (1990) 358.
[14] N. Rinaldi, IEEE Trans. Electron. Devices 42 (6) (1995) 1126.
[15] C.R. Selvakamur, J. Appl. Phys. 56 (12) (1984) 3476.
[16] PC1D 5.1 User's manual P. Basore, D. Clugston, University of New South Wales, 1997.